Proton Irradiation Platforms for Preclinical Studies of High-Dose-Rate (FLASH) Effects at RARAF

Authors: Grilj, V., Buonanno, M., Welch, D., and Brenner, D. J.

Source: Radiation Research, 194(6) : 646-655

Published By: Radiation Research Society

URL: https://doi.org/10.1667/RADE-20-00062.1

RADIATION RESEARCH **194**, 646–655 (2020)
0033-7587/20 $15.00

DOI: 10.1667/RADE-20-00062.1

Proton Irradiation Platforms for Preclinical Studies of High-Dose-Rate (FLASH) Effects at RARAF

V. Grilj,[1] M. Buonanno, D. Welch and D. J. Brenner

Center for Radiological Research, Columbia University Irving Medical Center, New York, New York

Grilj, V., Buonanno, M., Welch, D. and Brenner, D. J. Proton Irradiation Platforms for Preclinical Studies of High-Dose-Rate (FLASH) Effects at RARAF. *Radiat. Res.* 194, 646–655 (2020).

Limited availability of proton irradiators optimized for high-dose-rate studies makes the preclinical research of proton FLASH therapy challenging. We assembled two proton irradiation platforms that are capable of delivering therapeutic doses to thin biological samples at dose rates equal to and above 100 Gy/s. We optimized and tested dosimetry protocols to assure accurate dose delivery regardless of the instantaneous dose rate. The simplicity of the experimental setups and availability of custom-designed sample holders allows these irradiation platforms to be easily adjusted to accommodate different types of samples, including cell monolayers, 3D tissue models and small animals. We have also fabricated a microfluidic flow-through device for irradiations of biological samples in suspension. We present one example of a measurement with accompanying preliminary results for each of the irradiation platforms. One irradiator was used to study the role of proton dose rate on cell survival for three cancer cell lines, while the other was used to investigate the depletion of oxygen from an aqueous solution by water radiolysis using short intense proton pulses. No dose-rate-dependent variation was observed between the survival fractions of cancer cells irradiated at dose rates of 0.1, 10 and 100 Gy/s up to 10 Gy. On the other hand, irradiations of Fricke solution at 1,000 Gy/s indicated full depletion of oxygen after proton doses of 107 Gy and 56 Gy for samples equilibrated with 21% and 4% oxygen, respectively.

INTRODUCTION

In the field of radiation oncology, there is a continuous pursuit to improve the differential response between normal and tumor tissue. With the number of cancer survivors in the U.S. increasing each year (*1*), the importance of minimizing late adverse effects of radiation therapy is growing. In 2014 Favaudon *et al*. presented a novel approach to cope with radiation-induced toxicity to the normal tissue surrounding the irradiated tumor (*2*). This approach, known as FLASH therapy, consists of delivering a total dose in one fraction at dose rates exceeding 40 Gy/s. Studies indicated that by reducing the time interval for delivering a single dose fraction to tens or hundreds of milliseconds, detrimental radiation effects in mouse lung (*2*) and brain (*3, 4*) can be reduced, or even avoided, without sacrificing the local tumor control. However, despite strong preclinical evidence, exact molecular mechanisms behind the observed phenomenon are not well understood.

Progress in revealing the biological pathways that lead to the FLASH sparing effect is in part hampered by the limited availability of high-dose-rate irradiators to the research community. Appropriate machines should be able to deliver therapeutically relevant doses ($>$2 Gy) at dose rates of $>$40 Gy/s while keeping the irradiation times well in the sub-second range. Groups from Stanford (*5*) and Lund (*6*) have performed modifications on regular clinical linear accelerators (LINAC) that allowed them to successfully deliver electron beams at dose rates higher than 200 Gy/s. In both cases the authors presented a proof of concept for the upgrade to FLASH mode and it is not clear if, and for how long, these modified setups will remain available for use in radiobiological experiments.

Currently there are several published studies that have confirmed outstanding normal tissue sparing after FLASH irradiations with photon and electron beams (*2–4, 7, 8*). Whether similar effects can be elicited by other types of radiation is still unknown. Indeed, no *in vivo* data exist which support the manifestation of FLASH sparing effect with proton beams, but such data are highly relevant since the adoption of proton beams in radiotherapy is increasing worldwide. While the Varian FLASHForward Consortium of proton therapy facilities from Europe and the U.S. was established in 2017 with the goal of researching the clinical implementation of proton FLASH therapy, and simple technological developments were sufficient to adapt clinical proton beamlines for studies on small animals under FLASH conditions (*9*), there is still a need to develop proton FLASH irradiation platforms available exclusively to scientists.

[1] Address for correspondence: Center for Radiological Research, Columbia University Irving Medical Center, 630 W. 168th St., New York, NY 10032; email: vg2400@cumc.columbia.edu.

In the current work, we describe two irradiation platforms that were developed for FLASH studies with proton beams at the Radiological Research Accelerator Facility (RARAF) at Columbia University (New York, NY) (*10*). The platforms are optimized for high-dose-rate proton irradiations of thin (up to 300 μm) biological models and remain permanently available to the research community. The technical data regarding the experimental setups are followed by descriptions of two experiments that were performed at the FLASH irradiation platforms. In the first experiment, the clonogenic survival of three cancer cell lines irradiated at various dose rates was investigated. In the second experiment, the oxygen depletion from aqueous solution induced by short proton pulses was studied; this is important because the lack of oxygen was suggested to play an important role in inducing the FLASH sparing effect (*4, 11*).

MATERIALS AND METHODS

Two irradiation platforms were developed for investigating the FLASH effect with protons: the track-segment irradiator and the FLASH irradiator. Both platforms use a 5.5-MV Singletron accelerator (HVE Europa B.V., Amersfoort, Netherlands) as a source of energetic protons. The platforms were constructed on the same beamline, which emerges at 10.5° to the right after the switching magnet. The schematic drawing of the RARAF beamlines is provided elsewhere by Marino (*10*). The beam arrives horizontally at the FLASH irradiator end station located in the shielded horizontal (SH) area and vertically from below at the track-segment irradiation facility located in the shielded vertical (SV) area. All calibrations and experiments were done with protons having the highest achievable energy in vacuum of 5.5 MeV.

Track-Segment Irradiator

The track-segment platform was originally developed in 1976 at Brookhaven National Laboratory (BNL; Upton, NY) (*12*) and started in operation at the current location at Nevis Laboratories (Columbia University, Irvington, NY) in 1984 (*10*). It has since been extensively used for broad beam irradiations of thin biological targets (mainly cell monolayers) with ions having a precisely defined linear energy transfer (LET) (*13–16*). The operation of the platform is described in greater detail elsewhere (*12, 17, 18*). Briefly, the irradiation protocol consists of rotating a flat irradiation wheel with custom-made sample dishes over the vertical ion beam. The beam is defocused to homogeneously cover the 6 mm × 20 mm vacuum exit aperture. A 2.9-μm-thick havar foil serves as an interface between the vacuum system and the atmosphere. One of the advantages of this platform is a well-designed dosimetry protocol based on three detectors: a proportional counter that measures the average LET of ions in 6 μm of tissue; a surface barrier silicon diode that measures the total beam energy at the target; and an ionization chamber that measures dose to tissue and the dose rate. The proportional counter and the ionization chamber are filled with the methane-based tissue-equivalent gas. All three detectors are mounted on the dosimetry wheel which is exposed to the beam prior to the irradiation of samples. The beam monitor, which is a part of the motor drive system that controls the speed of the wheel rotation, continuously monitors the instantaneous beam current by wiping off a small portion of the beam penumbra. During the dosimetry protocol, the ionization chamber is scanned over the beam exit window instead of the sample dish. Scanning is done with the stepper motor which is controlled by the custom made software. The motor moves the chamber step by step, waiting at each position until the appropriate number of monitor counts is registered. In that way the monitor chamber signal defines the rotation speed of the wheel. Initial number of monitor counts per step can be defined within in the software. After the entire ionization chamber moves over the beam the deposited dose is calculated from the electric charge produced inside the chamber and a correction factor is defined to correct the number of counts per step to obtain the desired dose (input given to the software, usually 2–5 Gy). The chamber is then scanned over the beam with the new number of monitor counts per step and the correction factor is determined again as a ratio between the desired and the measured dose. The procedure is repeated until the correction factor becomes less than 1% different from unity. When this requirement is achieved, the dosimetry protocol is considered to be successfully finished and the rotation speed of the wheel is calibrated in terms of monitor counts/step/Gy. Now the wheel with sample dishes can be positioned on the irradiator and the irradiation protocol started. As an input, the operator provides the doses that should be delivered. The number of monitor counts per step is calculated for each dose according to the result of the dosimetry protocol. Sample dishes are scanned over the beam in the exact same way as the ionization chamber was. Irradiation of each sample dish starts by positioning the dish outside of the exposure field near the edge of the beam exit window. The wheel then rotates step by step, pausing at each position until the appropriate number of monitor counts is registered. The beam current and consequently the dose rate can be easily manipulated by changing the settings of the ion source and/or tuning the defocusing quadrupole magnets which blow up the beam size to homogeneously cover the whole exit window. As the dose rate is increased, it will take less time to reach the same number of monitor counts and the faster rotation speed will be required. The highest dose rate that can be used for irradiations at the track-segment irradiator is actually limited not by the available beam intensity, but by the maximum rotation speed that can be achieved with the current motor drive system. For instance, with the standard beam exit window (6 mm width), the motor system saturates at dose rates of approximately 10 Gy/s. To be able to perform irradiations at even higher dose rates (over 100 Gy/s), we had to narrow the exit aperture down to prevent the saturation of the wheel motor drive system. As a solution, a 100-μm thick nickel foil with a 1-mm-wide line opening was mounted on top of the current exit aperture.

Dosimetry assessment with films. The response of the Gafchromic™ EBT3 films (Ashland™ ISP, Wayne, NJ) was previously shown to be dose-rate independent up to the 10^6 Gy/s range (*19*), which makes these films suitable for use as absolute dosimeters in FLASH experiments. We compared the actual doses received by the film at various dose rates with the preset dose values defined within the irradiation protocol for the track-segment program to check the dose accuracy of the track-segment irradiator in FLASH mode. Unlaminated EBT3 films, which are one half the thickness of regular EBT3 film and have an exposed active region on one side, were irradiated with the same set of doses (1, 2, 5, 10, 15 and 20 Gy) at instantaneous dose rates of 0.1, 1, 10 and 100 Gy/s. Three pieces of film were irradiated with each dose/dose rate combination. Unlaminated films were used to reduce the energy loss of ions before they reach the active layer since the active layer is directly exposed. The active layer of unlaminated film is also one half the thickness compared to the active layer on the standard EBT3 version. These features of unlaminated film help to keep the LET of the proton beam far from the Bragg peak and nearly constant throughout the active layer. This was important since the signal from Gafchromic films depends on the LET (*20–24*). Irradiation, handling, scanning and readout of the films were done exactly as described elsewhere by our group (*20*). The net optical density change, netOD, was used to describe the darkening of the films in the red channel and was calculated as:

$$netOD = -log\left(\frac{\overline{PV} - \overline{PV}_{dark}}{\overline{PV}_0 - \overline{PV}_{dark}}\right), \quad (1)$$

where $\overline{PV}$ and $\overline{PV}_0$ are the mean pixel values of exposed and unexposed films, respectively, averaged over the selected regions of

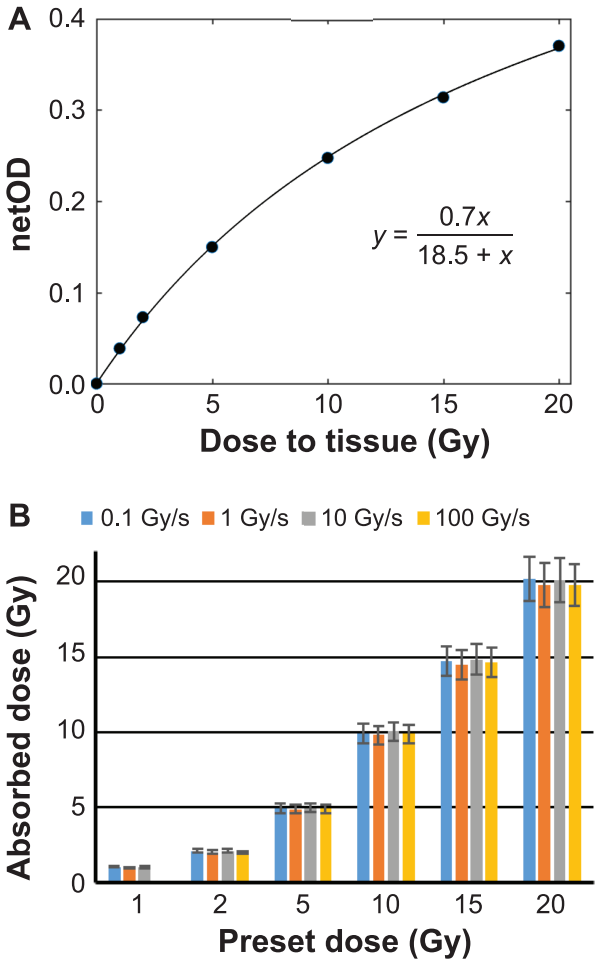

FIG. 1. Panel A: Change in optical density in the red channel of unlaminated EBT3 film as a function of absorbed dose to tissue after 6 Gy/min proton irradiation. The obtained nonlinear fit was used as a general calibration for the film dose response. Panel B: Comparison of measured absorbed doses and preset dose values defined within the track-segment irradiation protocol for various dose rates. Error bars represent the standard deviation in absorbed dose determined with films as described in the section, Dosimetry assessment with films.

interest (1 × 1 cm region in the center of the film), and $\overline{PV}_{dark}$ is the background scanner reading. Scanner reproducibility and film uniformity were taken into account by adding 1% error to uncertainty, σ_{netOD}, that was determined by propagating the errors $\sigma_{\overline{PV}}$, $\sigma_{\overline{PV}_0}$ and $\sigma_{\overline{PV}_{dark}}$. Final netOD values were determined by averaging over the three readings obtained from films exposed to the same radiation conditions (dose/dose rate). Dose-response data obtained at the lowest dose rate of 0.1 Gy/s were fitted to the expression suggested by the film manufacturer (Fig. 1A):

$$netOD = \frac{aD}{b + D}, \tag{2}$$

where *netOD* represents the change in optical density, D represents the dose and a and b are the calibration coefficients. This calibration was applied to translate the netOD values into absorbed dose for all other dose rates. It should be emphasized that due to the LET dependence, the obtained calibration coefficients are valid only for the LET value in tissue of 9 keV/μm, as measured with the tissue-equivalent proportional counter. The layers between the havar vacuum window and the target plane are similar at both irradiation platforms for FLASH studies, causing the energy of the beam reaching the samples to differ by less than 1%. Therefore, the calibration obtained at the track-segment irradiator with advanced dosimetry protocol can be applied as well to the films irradiated at the FLASH irradiator.

Biological application: Clonogenic survival of cancer cells. The first FLASH irradiations of biological samples at the track-segment irradiator were performed with the aim of investigating the role of proton dose rate on the survival of two human and one mouse cancer cell lines. Human lung adenocarcinoma cells A549 (CCL-185; ATCC®, Gaithersburg, MD) were grown in Dulbecco's Modified Eagle medium (DMEM) supplemented with 12% fetal calf serum (FBS); human myelogenous leukemia cells HAP1 (C859 Horizon) were grown in Iscove's Modified Dulbecco medium (IMDM) supplemented with 10% FBS; mouse mammary adenocarcinoma cells (TSA; kindly donated by Dr. Sandra Demaria from Cornell University, New York, NY) were grown in DMEM supplemented with 10% FBS. For every cell line, the media also contained 100 U/ml penicillin and 100 μg/ml streptomycin. Flasks were stored at 37°C in an incubator filled with humidified air and 5% CO_2. Cell survival was determined using the standard colony formation assay (*25*). Briefly, cells were trypsinized within 5–10 min of exposure, suspended in growth media, counted, diluted and seeded in 100-mm dishes with numbers resulting in ~100 clonogenic cells per dish. Three replicates were done for each data point. After 10-day incubation, the cells were rinsed with phosphate buffered saline (PBS), fixed in 95% ethanol and stained with crystal violet. Macroscopic colonies with more than 50 cells were scored as survivors. Measured survival values were corrected for the system plating efficiency which ranged from 60% in the case of the A549 cells to 70% for the TSA cells, as measured with nonirradiated controls.

FLASH Irradiator

The FLASH irradiator was assembled as an extension to the horizontal part of the track-segment beamline. Approximately 1 m after the switching magnet that directs the ions towards the appropriate beamline, monoenergetic protons encounter a beam deflector comprised of two parallel 0.6-m-long metal deflector plates mounted 3 cm apart. Deflector plates are directly coupled to the output of the TREK® voltage amplifier unit (Lockport, NY) with an amplification factor of 100. The amplifier is run with an offset voltage of 1,000 V applied between the plates. The transverse momentum introduced by this electric field bends the trajectory of the beam enough to make protons hit the slits closed down to 3 mm around the middle of the beam optical axis and positioned approximately 4 m behind the deflector. To expose the samples to intense proton beam pulses, the deflector gets discharged by sending a square 10-V pulse generated by a waveform generator (B&K Precision Corp., Yorba Linda, CA) to the TREK unit. The duration of the discharging pulse is equal to the beam-ON time and, in combination with dose rate, determines the total dose that will be delivered. When the deflector is discharged, the beam can reach the end of the beamline and exit into the atmosphere through a 2.9-μm-thick havar foil. The foil is suspended over the 10-mm-wide exit aperture and is strong enough to withstand a one-bar pressure difference applied over that area. An ionization chamber, placed between the havar foil and the target, is used as an online monitor of proton current. Samples are mounted on a motorized stage that moves in a 2D plane perpendicular to the beamline axis. The motion of the stage is controlled by the computer software (AMICron version 5.81) paired with a motor controller (Semprex® Corp., Campbell, CA). A standard webcam (Logitech, Lausanne, Switzerland) is used for positioning of the samples in front of the beam. Sample holders are custom designed and manufactured according to the needs of each experiment, which makes the irradiation platform easily adaptable to samples of various shapes and biological complexity. The end-station is described further in Results and Fig. 3.

Dosimetry protocol. The dosimetry protocol at the FLASH irradiator platform is based on two devices: a thin parallel plate ionization chamber and unlaminated Gafchromic EBT3 films. The

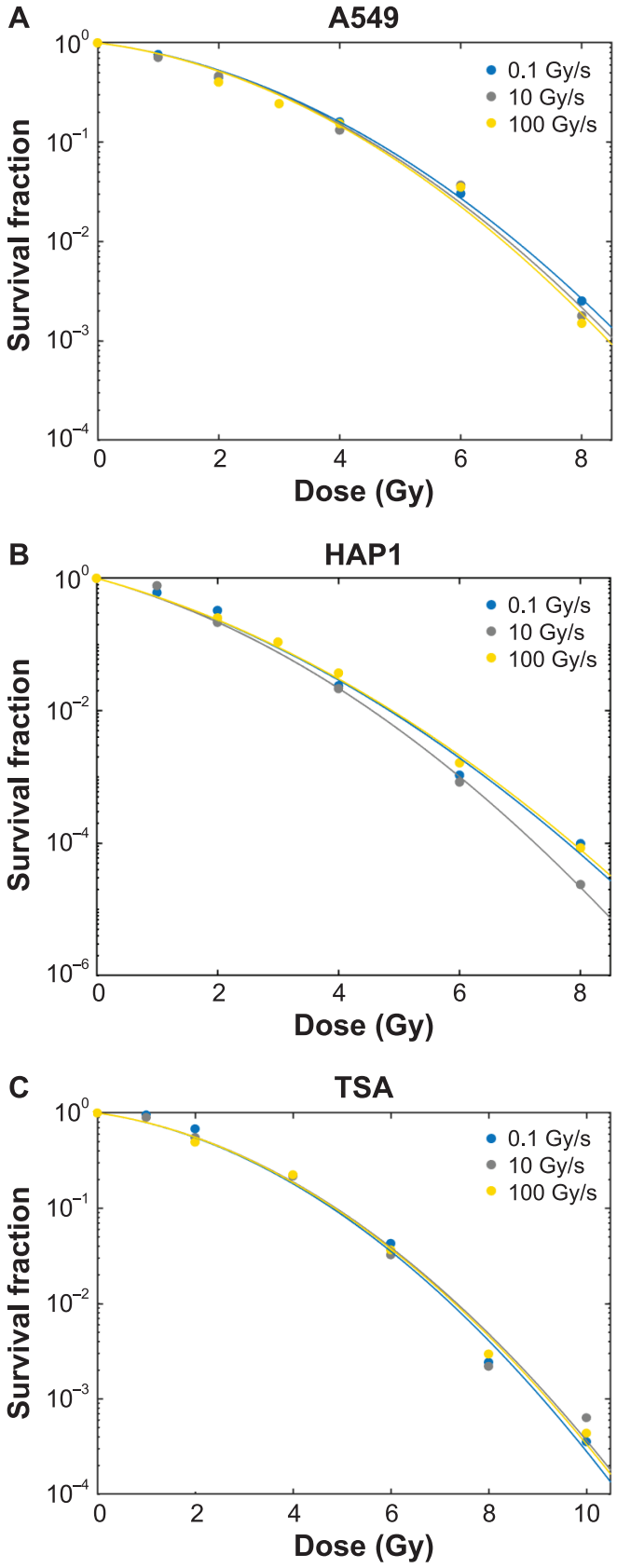

FIG. 2. Survival curves for A549, HAP1 and TSA cancer cell lines irradiated at the track-segment irradiator with dose rates of 0.1, 10 and 100 Gy/s.

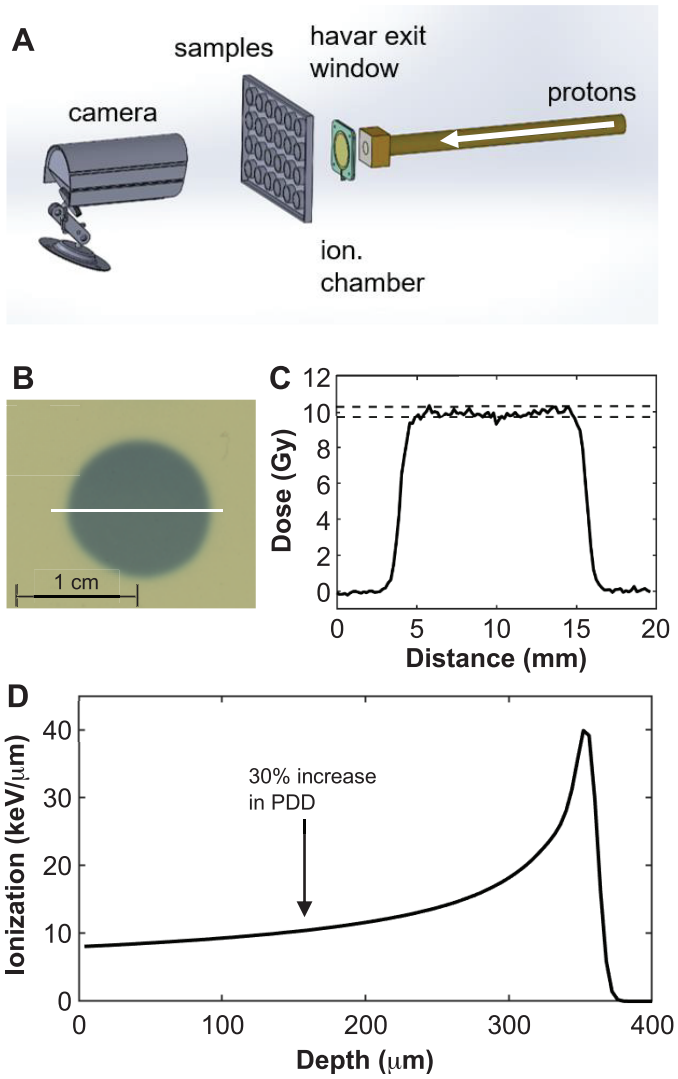

FIG. 3. Panel A: Schematic image of the FLASH irradiator end-station. Panel B: The shape of the exposure area of the FLASH irradiator as recorded by irradiating an EBT3 film with a dose of 10 Gy. Panel C: Horizontal dose profile along the white line shown in panel A with ±3% dose limits shown by intermittent lines. Panel D: The depth-dose profile of 5.03-MeV protons in water simulated by TRIM Monte Carlo software. Percentage depth dose (PDD) increases by 30% at a depth of 160 μm.

ionization chamber is used to set the dose rate and to monitor the beam current during the experiment while films are used to confirm that the appropriate dose was delivered to the target. Before the actual irradiation, the sample is moved away from the irradiation field and the beam is allowed to propagate unobstructed and reach the ionization chamber mounted in air, 2 mm apart from the havar foil. With continuous beam on, a current measured by the ionization chamber is directly proportional to the instantaneous proton dose rate. The beam intensity is then tuned until the desired reading from the ionization chamber is achieved. Characteristics and the calibration of the ionization chamber are described in the section on dose-rate measurements, below. Once the dose rate is set, the beam is deflected by the offset voltage on the TREK unit. A sample can be positioned in front of the exit aperture and irradiated by pressing the trigger button on the waveform generator. The duration of the voltage pulse used to discharge the deflector plates depends on the required dose and can be easily controlled in the settings panel of the waveform generator.

1. Absolute dosimetry with films. Doses that are delivered by high-intensity proton pulses during an experiment are verified by unlaminated Gafchromic EBT3 films to ensure that the LET in the active layer of the film remains nearly constant. A piece of film is mounted on the stage together with samples and positioned so that the active layer and the surface of the sample are at the same distance from the vacuum window. Each film is irradiated three times for each dose rate/pulse duration combination that is used within the experiment. Irradiated films are handled and processed as described above, in the section on track-segment film dosimetry. A dose-response calibration curve obtained with the track-segment facility at a dose rate of 0.1 Gy/s was used to read the dose from the film signal. An LET correction of the form,

$$k_{LET} = \frac{\overline{LET}_d}{9keV/\mu m}, \tag{3}$$

with $\overline{LET}_d$ being a dose-averaged LET in the sample, is required for thicker samples to account for an increase in LET throughout the sample. The value of 9 keV/μm corresponds to the LET in tissue that was used to obtain the calibration curve at the track segment. The final dose is determined as the mean of three film readings obtained with the same pulse conditions while dose uncertainty is obtained by propagation of the corresponding errors.

2. Dose-rate measurements with ionization chamber. Dose rate of the proton beam is monitored online by the custom-made ionization chamber, which consists of two parallel circular electrodes made from 0.1-μm-thick titanium microfoil (Goodfellow Corp., Coraopolis, PA) supported by 3.5-μm-thick mylar. Electrodes are fixed 3 mm apart and the interior of the chamber is filled with methane-based tissue-equivalent gas at ambient pressure. The ionization current generated by traversing protons is read with the electrometer and normalized to standard pressure and temperature by applying the correction factor,

$$k_{p,T} = \frac{(273.2 + T)}{293.2} \times \frac{760}{P}, \tag{4}$$

where T is the temperature in degrees Celsius, and P pressure in mmHg at the time of measurement. The corrected current reading is independent from the ambient conditions and was calibrated in terms of the dose rate with the help of the unlaminated EBT3 film. This was done by exposing films to proton pulses of various duration while keeping the current through the ionization chamber fixed. Analysis of the irradiated films provided the relationship between the pulse length and the absorbed dose with dose rate as a factor of proportionality. The procedure was repeated for several dose rates spanning a range of five orders of magnitude (from 0.02 Gy/s to 1,000 Gy/s) while the lengths of the irradiation pulses were scaled to deliver approximately the same doses with different beam intensities. The obtained dose-rate calibration is again valid only for LET of 9 keV/μm. Experiments with thicker samples require LET correction, defined by Eq. (1).

Biochemical Application

1. The microfluidic flow-through system. An additional feature available at the FLASH irradiator is a microfluidic flow-through system that was manufactured to allow for larger volumes (up to 1 ml) of liquid samples to be irradiated with short-range protons. The system is convenient for experiments with blood samples, suspended cells or chemical solutions. It is based on a microfluidic device containing a 100-μm-deep and 1-mm-wide channel through which the sample is forced to flow by a standard syringe pump (New Era Pump Systems Inc., Farmingdale, NY). During the flow, media is exposed to a continuous beam of protons at a desired dose rate. The microfluidic device was fabricated using traditional Polydimethylsiloxane (PDMS) soft microfluidic fabrication methods (*26*), with the exception of our mold fabrication which was made using a craft cutter similar to the work by Taylor *et al.* (*27*). Briefly, we defined a pattern using AutoCAD® (AutoDesk® Inc., San Rafael, CA) which was then exported to a Silhouette Cameo® craft cutter (Silhouette America, Lindon, UT). The craft cutter was used to cut a piece of clear polyester double-sided tape (Adhesives Research® Inc., Glen Rock, PA). After cutting the desired pattern, the liner was removed from one side, leaving a total thickness of approximately 100 μm, and the pattern was adhered to a glass slide to act as a negative mold. The mold was covered with uncured PDMS and allowed to cure overnight at room temperature. The cured PDMS was released from the mold, inlet and outlet holes were punched using a 1.25-mm biopsy punch, and the PDMS structure was sealed to a 30-μm-thick piece of glass (Schott, Elmsford, NY) using oxygen plasma bonding. The ring structure used for this work had an outer diameter of 4.5 mm and an inner diameter of 3.5 mm, thus with a 100-μm height of the channel the total volume in the target area was approximately 2.5 μl.

2. Irradiations of Fricke solution at different oxygen concentrations. The microfluidic flow-through system described above is convenient for investigating proton beam-induced oxygen depletion in water-based solutions at FLASH dose rates. To demonstrate this, we exploited the dependence of the dose response of the Fricke chemical dosimeter (*28–30*) on the presence of oxygen in the solution. One liter of Fricke solution was prepared by mixing 0.392 g of ammonium ferrous sulfate hexahydrate $[(NH_4)_2Fe(SO_4)_2]$, 0.058 g of sodium chloride [NaCl] and 0.4 *M* of sulfuric acid with ultra-pure distilled water (Invitrogen™, Carlsbad, CA). Dosimetric properties of the ferrous sulfate dosimeter are based on the radiolytic oxidation of ferrous (Fe^{2+}) to ferric (Fe^{3+}) ions and subsequent change in optical density (OD) at 303 nm (*28–33*). However, the yield of Fe^{3+} ions postirradiation is reduced if all of the molecular oxygen is consumed from the solution by the products of water radiolysis (*32, 34, 35*). Oxygen depletion during proton FLASH irradiation was studied with Fricke solutions containing 21% O_2 and 4% O_2. The higher oxygen content corresponds to atmospheric conditions, while the lower value was chosen as a representative of tissue conditions, although the partial pressure of O_2 varies significantly from organ to organ (*36*). Solutions with different O_2 concentrations were prepared from the same stock by equilibrating the samples at either room air (for 21% O_2 solution) or using a gas mixture containing 4% O_2 and 96% N_2. Before every exposure, the microfluidic channel was washed twice with fresh Fricke solution and dried by flushing the appropriate gas (air or 4% O_2 mixture) through the channel. A syringe pump was used to propel the Fricke solution in the microchannel, which was exposed to a continuous proton beam at 1,000 Gy/s. It should be noted here that due to the parabolic velocity profile across the channel width (1 mm), the maximum medium velocity in the middle of the channel is approximately 50% higher than the velocity near the channel edges (*37*). As a consequence, each irradiated sample was exposed to a distribution of doses. The final dose assigned to the sample was actually the average dose that corresponds to the product of the average flow rate (set by the syringe pump) and the LET-corrected dose rate. Average LET in the media required for the correction was calculated by Monte Carlo simulations described below. Doses used in the experiment ranged from 0 to more than 1,000 Gy. At every flow rate, three irradiated samples of 1-ml volume each were collected in vials and sealed. Samples were transferred into a quartz cuvette and read 24 h after irradiation using the Spectronic GENESYS 7 spectrophotometer (Thermo Electron Scientific Instruments LLC, Madison, WI) set to measure the absorbance at 303 nm. The same cuvette was used for all samples. During the sample exchange, the cuvette was washed twice with ultra-pure water.

For comparison, 1 ml of Fricke solution samples were X-ray irradiated [160 kVp, 1-mm-copper half-value layer (HVL), 0.3-mm copper filtering] at a dose rate of 8 Gy/min. Dosimetry was performed immediately prior to irradiation, using a NIST-traceable ionization chamber (Radcal®, Monrovia, CA) calibrated to air kerma. Readout of the irradiated samples was performed 24 h postirradiation, as described earlier.

3. Monte Carlo simulations. The LET of protons inside the microfluidic channel during the experiment with the Fricke dosimeter was determined from simulations done using the TRIM module of the Monte Carlo software SRIM (*38*). Protons with nominal energy of 5.4 MeV pass through a total of 2.9 μm of havar foil, 4 mm of air, 3 mm of methane-based tissue-equivalent gas, 30 μm of glass and 100 μm of Fricke solution which was represented with water. TRIM software was used to simulate the energy of the beam right before and after traversing the Fricke solution. The difference between those energies gives the energy deposited in the solution. The average LET was defined then as a ratio of the deposited energy and the thickness of the media (100 μm).

RESULTS

Performance of the Track-Segment Irradiator

The track-segment irradiator is optimized for irradiations of cell monolayers. Its dosimetry protocol measures dose, dose rate and LET of particles in the first several micrometers of tissue. With the exit aperture narrowed down to 1 mm, the track-segment irradiator is capable of delivering doses as small as 2 Gy at a dose rate of 100 Gy/s, which falls under the range for which the FLASH effect was observed with electron beams. Exposures at higher dose rates are also possible, but require a proportional increase of the lowest deliverable dose, which is limited by the maximum rotation speed of the wheel.

The performance of the irradiator at high dose rates was tested with unlaminated EBT3 films. The irradiation protocol was tuned to deliver the same set of doses at dose rates of 0.1, 1, 10 and 100 Gy/s. Figure 1A shows the comparison between the absorbed doses in tissue measured with films and the preset dose values defined in the control software. For all dose/dose-rate combinations the difference between delivered and preset doses is less than 3%, confirming that the irradiator, with its standard dosimetry and irradiation protocols, can be reliably used for irradiations at high dose rates.

Dose-response data obtained for the lowest dose rate of 0.1 Gy/s were used to calibrate the film (Fig. 1B). Data were fitted to Eq. (2) and the resulting fitting parameters ($a = 0.7$, $b = 18.5$) were used for transferring the netOD values into dose for all films irradiated at track segment and the FLASH irradiator.

Survival of cancer cells. In our previously published work on the biological effects of proton FLASH radiation in normal cells, we investigated the role of proton dose rate on the survival of normal lung fibroblasts, IMR90 (*39*). Here, we focused on a similar experiment involving three cancer cell lines. Figure 2 shows the relationship between the survival fraction and the absorbed dose for human A549 and HAP1 and mouse TSA cells that were proton irradiated at dose rates of 0.1, 10 and 100 Gy/s. To analyze the data, survival fraction (SF) values were natural log (ln) transformed. The nonlinear regression was applied to fit the ln(SF) versus dose relationship to the second-order equation:

TABLE 1
Alpha and Beta Coefficients Obtained by Nonlinear Fit of Survival Data to Standard Linear-Quadratic Model

	A549		HAP1		TSA	
Dose rate (Gy/s)	α	β	α	β	α	β
0.1	0.17	0.071	0.57	0.079	0.17	0.065
10	0.16	0.074	0.53	0.079	0.16	0.062
100	0.16	0,076	0.56	0.076	0.19	0.063

$$\ln(\mathrm{SF}) = -\alpha D - \beta D^2, \tag{5}$$

where α and β are the standard coefficients of the linear-quadratic model. Calculated α and β values are shown in Table 1. As shown in Fig. 2, for each cell line there is no difference in the survival trends regardless of the dose rate. Consequently, the fitted α and β values show no significant variation among different dose rates, as tested using the Student's *t* test.

The FLASH Irradiator

Contrary to the track-segment platform, where the samples are irradiated by scanning the sample dish over the beam, the FLASH irradiator delivers sub-second proton pulses to the whole target area at once. The diameter of the exposure field is limited by the exit aperture and measures approximately 12 mm, as can be seen by examining the piece of unlaminated EBT3 film exposed to one FLASH pulse delivering 10 Gy (Fig. 3A). Dose is delivered homogeneously over this whole area (Fig. 3B). The energy of the beam at the target plane is equal to 5.03 MeV as simulated by SRIM. Protons with this energy stop in 360 μm of tissue (Fig. 3C). However, due to the increase in stopping power towards the end of the ion range, absorbed dose in tissue at a depth of 160 μm is already 30% higher than the entrance dose. Thus, the variation in dose with depth should be taken into account when planning for the experiment.

The custom-made ionization chamber used for monitoring the beam current during the experiment was tested for possible ion recombination at high dose rates. This was done by measuring the ionization current in the chamber at different operating voltages during exposure to beam at dose rates of 100 Gy/s and 1,000 Gy/s. The current-voltage (I-V) characteristics showed a plateau region in both cases, starting at approximately 300 V for 100 Gy/s and 800 V for 1,000 Gy/s (Fig. 4A). Based on these results, 1,000 V was used as a standard operating voltage for the ionization chamber. At this voltage, the recombination of ions in the ionization chamber was estimated to be less than 1% at 1,000 Gy/s using the 2-voltage method (*40*).

Dose rate measurements. During an experiment at the FLASH irradiator, the instantaneous dose rate is measured by the custom-made ionization chamber. To calibrate the chamber, we measured dose as a function of a pulse

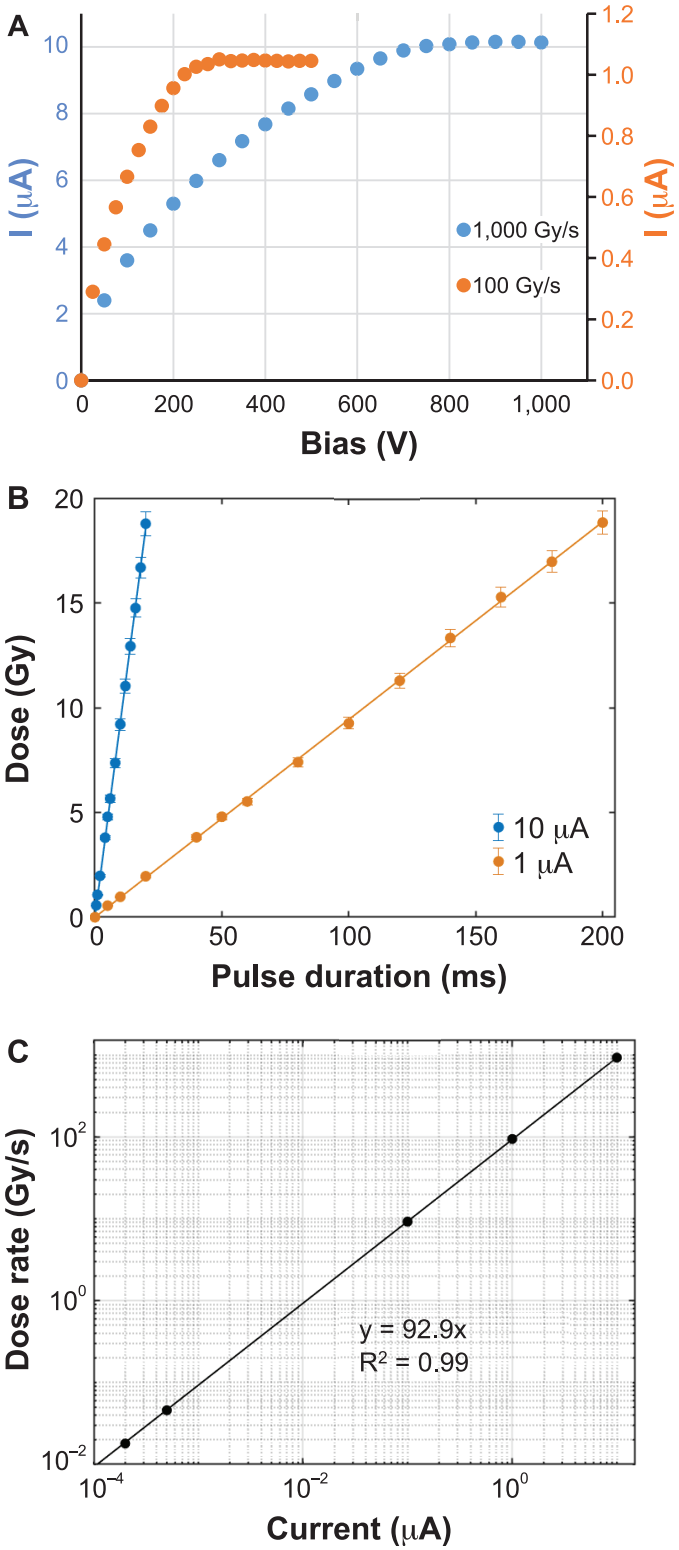

FIG. 4. Panel A: I-V characteristic of the custom-made ionization chamber at dose rates of 100 Gy/s and 1,000 Gy/s. Panel B: Dependence of the absorbed dose on the time duration of radiation pulses at the FLASH irradiator for corrected ionization chamber current readings of 1 and 10 μA. Panel C: Dose-rate values that correspond to several corrected ionization chamber current readings. All lines represent linear fits to data. Error bars represent standard deviation of the absorbed dose values determined using films as described in the section on dosimetry assessment with films.

duration at different electrometer readings. Figure 4B shows an example of such relationships for electrometer readings of 1 μA and 10 μA (dose rates of approximately 94.3 Gy/s and 928 Gy/s, respectively). Corresponding dose rates are equal to the slopes of the plotted relationships. Figure 4C shows calculated dose-rate values for ionization currents spanning six orders of magnitude. Linear fit of data points in Fig. 4C yielded a final dose rate calibration of (92.9 ± 0.2) Gy/s/μA.

Measurements of oxygen depletion by water radiolysis. The Fricke ferrous dosimeter was used to investigate depletion of dissolved oxygen by short intense pulses of proton radiation. Figure 5A and B shows the change in the absorbance of the Fricke solution equilibrated either at room air or with the gas mixture consisting of 4% O_2 and 96% N_2, respectively as a function of the average dose delivered at 1,000 Gy/s. It is evident that the initial rate of increase of absorbance becomes less steep after a certain dose. The rate of the increase of absorbance at low doses (<80 Gy for 21% O_2 and <40 Gy for 4% O_2) and high doses (>120 Gy for 21% O_2 and >70 Gy for 4% O_2) was determined by linear regression. Fitting results are shown in Fig. 5 as well. It is likely that the intersection of linear fits at low and high doses gives a dose value after which all oxygen gets depleted and consequently, the trend of change in absorbance breaks towards a lower rate. For Fricke solution equilibrated with 21% O_2 breaking occurs at a dose of 107 Gy, while for the solution equilibrated with 4% O_2 this effect occurs at a dose of 56 Gy. For comparison, samples taken from the same stock solution that received X-ray irradiation at low dose rates of 8 Gy/min show no break in response up to 600 Gy (Fig. 5C). After 800 Gy the response of the Fricke dosimeter saturates.

DISCUSSION

In this work we have presented two experimental platforms optimized for proton FLASH studies with thin biological models. The vertical proton beam at the track-segment irradiator is especially convenient for irradiations of cell monolayers since it allows for the presence of the cell media during the exposure. Dose rates higher than 100 Gy/s can be achieved at this platform. The maximum dose rate is determined by the limitations in rotation speed of the irradiation wheel and the lowest dose that has to be delivered. The track-segment facility has a well-designed and tested dosimetry protocol, which not only calibrates the irradiator in terms of dose, but also measures the LET of particles in a thickness corresponding approximately to a thickness of a living cell (Fig. 1). The first biological experiments performed at the track-segment irradiator in upgraded FLASH mode showed no dependence of cell survival on the proton dose rate over 0.1 to 100 Gy/s range for three cancer cell lines: two human (A549 and HAP1) and one mouse (TSA) (Fig. 2). It should be emphasized that the cells were kept at 21% O_2 during both incubation and

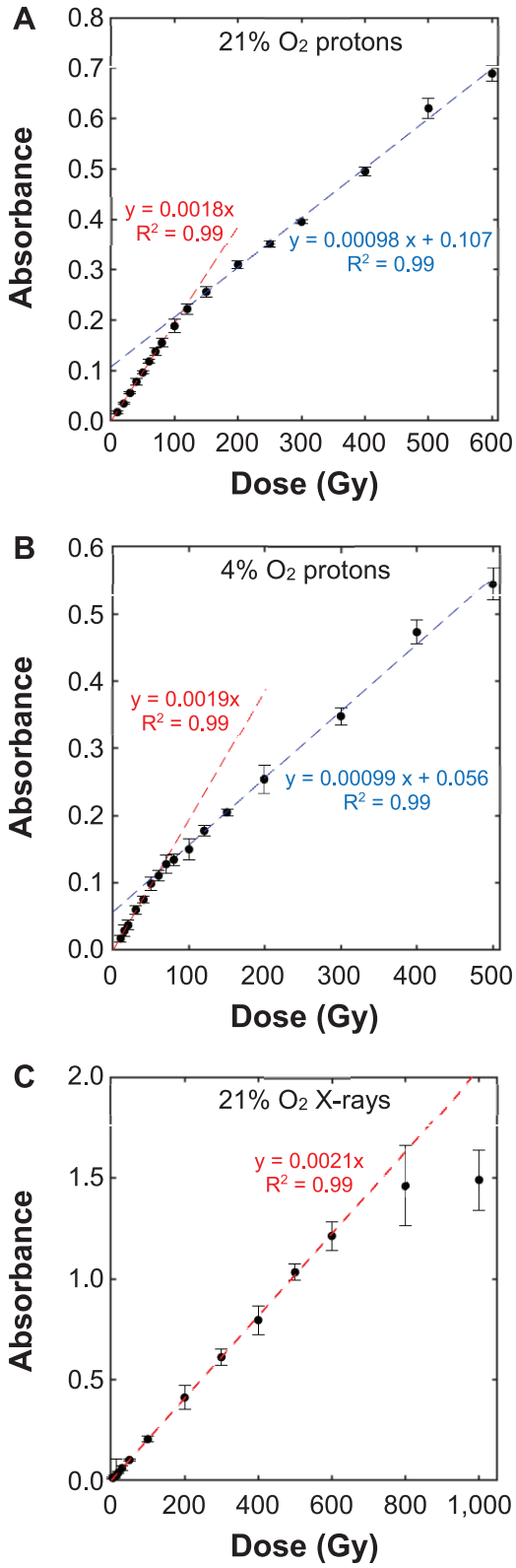

FIG. 5. Measured absorbance of the Fricke solution as a function of dose for samples equilibrated with 21% O_2 (panel A) or 4% O_2 (panel B) and proton-irradiated at a dose rate of 1,000 Gy/s. Panel C: Samples equilibrated with 21% O_2 X-ray irradiated at a dose rate of 8 Gy/min. Dashed lines represent linear fits to data at low (red) and high (blue) doses. The corresponding fitting results are shown inside the graphs. Black arrows indicate doses at which the breaking from the linear trend in the response occurs. Error bars represent standard errors of the mean.

irradiation. This consideration is important to bear in mind, since several authors have claimed that the radiation-induced depletion of oxygen is the main factor driving the FLASH sparing effect of normal tissues (*4, 11*). It is possible that the amount of oxygen in this study was too high to reach the full depletion with the highest applied dose of 10 Gy, and subsequently no difference in survival rates was observed. Moreover, the measured dose response of the Fricke dosimeter at high dose rates indicates that a dose in the range of 100 Gy is required to fully deplete the oxygen dissolved in aqueous solution equilibrated with 21% O_2 (Fig. 5). Survival studies under different oxygen levels are warranted to resolve the effect of oxygen on cell survival at FLASH dose rates.

The second platform for high-dose-rate experiments, the FLASH irradiator, is capable of delivering dose rates as high as 1,000 Gy/s to a circular area with a diameter of 12 mm (Fig. 3). Locally designed and manufactured sample holders make the platform easily customizable to samples of different shapes and sizes. The FLASH irradiator has been used in experiments with cells and 3D tissue models (*39*), but can be easily adapted for irradiations of mouse ear and skin. The main limitation of the platform is the range of ions in tissues. Protons accelerated to the highest beam energy that can be reached with the current accelerator stop in 360 μm of water. Moreover, the inhomogeneity in depth-dose distribution, which results from the gradual increase in stopping power towards the end of range, depends on the sample thickness and should be considered prior to every experiment. In general, the target that is being irradiated should not be thicker than 300 μm to avoid the placement of the Bragg peak inside the irradiated volume. Dosimetry protocol at FLASH irradiator is based on the use of both radiosensitive films and a custom-made transmission ionization chamber. Linearity of the chamber response with dose rate (beam current) was confirmed over five orders of magnitude with negligible ion recombination at high-beam intensities (Fig. 4B). Irradiations of samples in a liquid phase (chemical solutions, cell suspensions, blood samples) are possible with the use of the microfluidic flow-through system. Because of the limited ion range, the maximum volume of liquid that can be exposed to the beam at once is in the range of several microliters. The flow-through system allows for 1 ml or even larger volumes of irradiated media to be collected in a reasonable time (minutes or tens of minutes, depending on the dose). The system was applied in experiments with a Fricke dosimeter aiming to investigate the depletion of dissolved oxygen by water radiolysis (Fig. 5). Linearity in the response of the Fricke dosimeter with dose implies that, despite the inhomogeneous flow rate profile, the concept of the average dose delivered to the liquid sample that flows through an irradiation field is valid and does not introduce additional errors into dosimetric considerations. On the other hand, the response of the Fricke dosimeter exhibited a distinct change at a point which was dependent on the dissolved oxygen concentra-

tion when using a dose rate of 1,000 Gy/s. This breaking point likely indicates the dose at which oxygen is fully depleted from the solution. With no oxygen remaining, the yield of Fe^{3+} ions, and consequently the rate at which the absorbance of the irradiated solution, changes with dose decreases. This occurs at a lower dose for samples that were equilibrated with 4% oxygen compared to those saturated with room air (21% O_2). Results of linear regression for absorbance versus dose relationships show that the rates at which absorbance increases before and after the breaking point are independent of the starting oxygen concentration in solution. Also, calculated slope values indicate that the yield of Fe^{3+} ions in oxygenated solution is approximately twice as large as the same yield in anoxic solution. This is in very good agreement with published radiolytic yields of Fe^{3+} ions after ^{60}Co irradiations, which for an aerated solution is equal to 15.5 ions per 100 eV and for an anoxic solution is 8.2 ions per 100 eV (*34*). However, even in the case of the low oxygen concentration, the dose of 56 Gy, required to fully deplete the oxygen from the solution, is much higher than that required to induce the FLASH effect (*2–4, 7, 8*). Nevertheless, there are several details worth noting here. First, despite filling the whole flow-through system with gas mixture containing 4% O_2, it is possible that some exchange of oxygen between the tubing/microfluidic channel and the passing solution occurred during the irradiations. This would increase the actual oxygen concentration and result in the breaking occurring at a higher dose. Second, as mentioned earlier, the oxygen concentration varies across different tissues or even within different areas of the same tissue. For example, the mean oxygen concentration in the mouse brain was shown to be approximately 3% with some regions having as low as 50% of that amount (*41*). Consequently, doses much lower than 50 Gy might be sufficient to consume significant amounts of oxygen from those regions. Third, it is not clear how the chemical composition of the tissue influences the radiolytic oxygen depletion. Clearly, the Fricke solution is a fairly simplified aqueous solution without free radical scavengers that are usually found inside the cell and which compete with molecular oxygen in reacting with the products of water radiolysis. In the end, the proton beam used in these experiments has a time structure that is very different from the electron beam produced by a linear accelerator. Proton pulses used in this work have a continuous flow of ions during the whole beam-on time, while the electron beams that revealed the FLASH effect were bunched in time and consisted of a number of microsecond pulses with dose rates in each pulse exceeding 10^5 Gy/s. Nevertheless, in both cases the dose is delivered within milliseconds, which is short enough to prevent any reoxygenation during exposure so it is questionable whether the microstructure of the beam can influence the amount of consumed oxygen at such short time scales.

With all these considerations, we can conclude that our data do not support the assumption of full depletion of oxygen dissolved in water at proton doses as low as 10 or 20 Gy delivered at a homogeneous dose rate of 1,000 Gy/s; however, caution should be exercised when attempting to extrapolate this conclusion to intracellular media and other radiation modalities with similar average dose rates but possibly different beam microstructures.

Received: February 26, 2020; accepted: July 31, 2020; published online: September 14, 2020

REFERENCES

1. Miller KD, Nogueira L, Mariotto AB, Rowland JH, Yabroff KR, Alfano CM, et al. Cancer treatment and survivorship statistics. CA Cancer J Clin 2019; 69:363–85.
2. Favaudon V, Caplier L, Monceau V, Pouzoulet F, Sayarath M, Fouillade C, et al. Ultrahigh dose-rate FLASH irradiation increases the differential response between normal and tumor tissue in mice. Sci Transl Med 2014; 6:245ra93.
3. Montay-Gruel P, Petersson K, Jaccard M, Boivin G, Germond JF, Petit B, et al. Irradiation in a FLASH: Unique sparing of memory in mice after whole brain irradiation with dose rates above 100 Gy/s. Radiother Oncol 2017; 124:365–9.
4. Montay-Gruel P, Acharya MM, Petersson K, Alikhani L, Yakkala C, Allen BD, et al. Long-term neurocognitive benefits of FLASH radiotherapy driven by reduced reactive oxygen species. Proc Natl Acad Sci U S A 2019; 116:10943–51.
5. Schuler E, Trovati S, King G, Lartey F, Rafat M, Villegas M, et al. Experimental platform for ultra-high dose rate FLASH irradiation of small animals using a clinical linear accelerator. Int J Radiat Oncol 2017; 97:195–203.
6. Lempart M, Blad B, Adrian G, Back S, Knoos T, Ceberg C, et al. Modifying a clinical linear accelerator for delivery of ultra-high dose rate irradiation. Radiother Oncol 2019; 139:40–5.
7. Montay-Gruel P, Bouchet A, Jaccard M, Patin D, Serduc R, Aim W, et al. X-rays can trigger the FLASH effect: Ultra-high dose-rate synchrotron light source prevents normal brain injury after whole brain irradiation in mice. Radiother Oncol 2018; 129:582–8.
8. Vozenin M-C, De Fornel P, Petersson K, Favaudon V, Jaccard M, Germond JF, et al. The advantage of FLASH radiotherapy confirmed in mini-pig and cat-cancer patients. Clin Cancer Res 2018; 25:35–42.
9. Patriarca A, Fouillade C, Auger M, Martin F, Pouzoulet F, Nauraye C, et al. Experimental set-up for FLASH proton irradiation of small animals using a clinical system. Int J Radiat Oncol 2018; 102:619–26.
10. Marino SA. 50 Years of the Radiological Research Accelerator Facility (RARAF). Radiat Res 2017; 187:413–23.
11. Spitz DR, Buettner GR, Petronek MS, St-Aubin JJ, Flynn R, Waldron TJ, et al. An integrated physico-chemical approach for explaining the differential impact of FLASH versus conventional dose rate irradiation on cancer and normal tissue responses. Radiother Oncol 2019; 139:23–7.
12. Rohrig N, Colvett R. Annual Report on Research Project, ERDA Report COO-3243-5. Charged-particle beams for radiobiology at RARAF. Springfield, VA: National Technical Information Service; 1976. p. 38–54.
13. Jones GD, Milligan JR, Ward JF, Calabro-Jones PM, Aguilera JA. Yield of strand breaks as a function of scavenger concentration and LET for SV40 irradiated with 4He ions. Radiat Res 1993; 136:190–6.
14. Kovalchuk O, Zemp FJ, Filkowski JN, Altamirano AM, Dickey JS, Jenkins-Baker G, et al. microRNAome changes in bystander three-dimensional human tissue models suggest priming of apoptotic pathways. Carcinogenesis 2010; 31:1882–8.
15. Hei TK, Komatsu K, Hall EJ, Zaider M. Oncogenic transfonnation

by charged particles of defined LET. Carcinogenesis 1988; 9:747–50.

16. Miller RC, Marino SA, Brenner DJ, Martin SG, Richards M, Randers-Pehrson G, et al. The biological effectiveness of radon-progeny alpha particles. II. Oncogenic transformation as a function of linear energy transfer. Radiat Res 1995; 142:54–60.
17. Colvett RD, Rohrig N. Biophysical studies with spatially correlated ions. 2. Multiple scattering, experimental facility, and dosimetry. Radiat Res 1979; 78:192–209.
18. Bird RP, Rohrig N, Colvett RD, Geard CR, Marino SA. Inactivation of synchronized Chinese Hamster V79 cells with charged-particle track segments. Radiat Res 1980; 82:277–89.
19. Jaccard M, Petersson K, Buchillier T, Germond JF, Durán MT, Vozenin MC, et al. High dose-per-pulse electron beam dosimetry: Usability and dose-rate independence of EBT3 Gafchromic films. Med Phys 2017; 44:725–35.
20. Grilj V, Brenner DJ. LET dependent response of GafChromic films investigated with MeV ion beams. Phys Med Biol 2018; 63:245021.
21. Martisikova M, Jakel O. Dosimetric properties of Gafchromic(R) EBT films in monoenergetic medical ion beams. Phys Med Biol 2010; 55:3741–51.
22. Vadrucci M, Esposito G, Ronsivalle C, Cherubini R, Marracino F, Montereali RM, et al. Calibration of GafChromic EBT3 for absorbed dose measurements in 5 MeV proton beam and 60Co gamma-rays. Med Phys 2015; 42:4678–84.
23. Castriconi R, Ciocca M, Mirandola A, Sini C, Broggi S, Schwarz M, et al. Dose-response of EBT3 radiochromic films to proton and carbon ion clinical beams. Phys Med Biol 2017; 62:377–93.
24. Reinhardt S, Wurl M, Greubel C, Humble N, Wilkens JJ, Hillbrand M, et al. Investigation of EBT2 and EBT3 films for proton dosimetry in the 4–20 MeV energy range. Radiat Environ Biophys 2015; 54:71–9.
25. Puck TT, Marcus PI. Action of x-rays on mammalian cells. J Exp Med 1956; 103:653–66.
26. Xia Y, Whitesides GM. Soft lithography. Angew Chemie Int Ed 1998; 37:550–75.
27. Taylor D, Dyer D, Lew V, Khine M. Shrink film patterning by craft cutter: complete plastic chips with high resolution/high-aspect ratio channel. Lab Chip 2010; 10:2472.
28. Fricke H, Hart EJ. Chemical dosimetry. New York: Academic Press; 1966.
29. Jayson GG, Parsons BJ, Swallow AJ. The mechanism of the fricke dosimeter. Int J Radiat Phys Chem 1975; 7:363–70.
30. Ross CK, Klassen N V, Shortt KR, Smith GD. A direct comparison of water calorimetry and Fricke dosimetry. Phys Med Biol 1989; 34:23–42.
31. Klassen N V, Shortt KR, Seuntjens J, Ross CK. Fricke dosimetry: The difference between G (Fe3+) for 60Co gamma-rays and high-energy x-rays. Phys Med Biol 1999; 44:1609–24.
32. Meesat R, Sanguanmith S, Meesungnoen J, Lepage M, Khalil A, Jay-Gerin J-P. Utilization of the ferrous sulfate (Fricke) dosimeter for evaluating the radioprotective potential of cystamine: Experiment and Monte Carlo simulation. Radiat Res 2012; 177:813–26.
33. deAlmeida CE, Ochoa R, Lima MC de, David MG, Pires EJ, Peixoto JG, et al. A feasibility study of Fricke dosimetry as an absorbed dose to water standard for 192Ir HDR sources. PLoS One 2014; 9:e115155.
34. O'Leary M, Boscolo D, Breslin N, Brown JMC, Dolbnya IP, Emerson C, et al. Observation of dose-rate dependence in a Fricke dosimeter irradiated at low dose rates with monoenergetic X-rays. Sci Rep 2018; 8:4735.
35. Stuglik Z. On the ''Oxygen in heavy-ion track'' hypothesis. Radiat Res 1995; 143:343.
36. Ortiz-Prado E, Dunn JF, Vasconez J, Castillo D, Viscor G. Partial pressure of oxygen in the human body: A general review. Am J Blood Res 2019; 9:1–14.
37. Gad-el-Hak M. MEMS Introduction and fundamentals. Boca Raton, FL: CRC Press/Taylor and Francis Group; 2006.
38. Ziegler JF, Biersack JP, Ziegler MD. SRIM, the Stopping and Range of Ions in Matter. SRIM Co. 2008.
39. Buonanno M, Grilj V, Brenner DJ. Biological effects in normal cells exposed to FLASH dose rate protons. Radiother Oncol 2019; 139:51–5.
40. Andreo P, Burns DT, Hohlfeld K, Saiful Huq M, Kanai T, Laitano F, et al. Absorbed dose determination in external beam radiation therapy: An international code of practice for dosimetry based on standards of absorbed dose to water. Technical report series (Vol. 398), IAEA. Vienna: International Atomic Energy Agency; 2000.
41. Lyons DG, Parpaleix A, Roche M, Charpak S. Mapping oxygen concentration in the awake mouse brain. Elife 2016; 5:e12024.